Dalton Transactions

Cite this: *Dalton Trans.*, 2011, **40**, 4800

www.rsc.org/dalton

COMMUNICATION

Fabrication of fluorescent silica–Au hybrid nanostructures for targeted imaging of tumor cells†

Feng Cao, Ruiping Deng, Dapeng Liu,* Shuyan Song, Song Wang, Shengqun Su and Hongjie Zhang*

Received 19th January 2011, Accepted 14th March 2011
DOI: 10.1039/c1dt10106d

Uniform "core-satellite" structured nanoparticles containing organic dye incorporated in the silica shell and fluorescence quenching Au nanoparticles have been synthesized with excellent fluorescent properties, and their targeted imaging application in tumor cells has been investigated.

Introduction

During the past two decades, owing to their significant potential to offer new opportunities for early diagnosis and therapeutics, extensive work has been carried out on the biomedical applications of nanostructured materials.[1] For example, dye-doped silica nanostructures have several advantages for optical imaging: (i) high photostability isolates dye molecules from the outside environment, arising from the silica coating during the nanoparticle preparation process, (ii) the luminescence intensity of one dye-doped silica nanoparticle is approximately 10^4 times higher than that of one dye molecule.[2] However their applications are somewhat limited by their potential toxicity.

In contrast, gold nanoparticles (NPs) have been widely used in biomedical imaging and diagnostic tests, because of their ease of preparation and bioconjugation, high contrast, large absorption coefficients, and more importantly, they have been variously described as non-toxic.[3] They have been used as tracers and the cellular trajectories change according to the biological signals added to the bulk material, again suggesting that gold particles themselves are non-toxic.[4] For all the biomedical applications mentioned above, combining these multiple discrete components into a single multifunctional nanoparticle could be useful in a variety of applications.[5] Experimental results demonstrate that it is particularly difficult, because gold nanostructures are known fluorescence quenchers and a gold shell will also limit photon transmittance.[6] So, how to make the Au encapsulated Rubpy-dye-doped silica ($DySiO_2$) NPs remain fluorescent is a key question. Herein, we describe a facile synthesis of a bifunctional nanocomposite system consisting of $DySiO_2$ nanospheres and Au NPs. Specifically, these "core-satellite" structured nanoparticles with excellent fluorescent properties contain an organic dye incorporated in the silica shell and fluorescence quenching Au NPs. We also investigated the biolabeling properties of $DySiO_2$–$(Au)_n$ NPs, namely their binding to cancer cells selectively and efficiently through modification of the aptamer. To the best of our knowledge, the present work is the first report on the synthesis of DNA-conjugated Au encapsulated organically modified silica nanoparticles for their robust targeting.

Results and discussion

First, $DySiO_2$ NPs with surface amine groups are synthesized by a modified literature method.[7] The obtained nanoparticles have a homogeneous size of 60 nm (Fig. 1a). Second, high-quality Au NPs used in this study are citrate-stabilized Au particles which are synthesized according to a previously reported procedure.[8] TEM analysis of these nanomaterials indicates they have a size distribution of 5.0 ± 1 nm (Fig. 1b). The core-satellite-like $DySiO_2$–$(Au)_n$ nanospheres are prepared *via* Au NPs adsorbed on the surface of $DySiO_2$ nanospheres through an electrostatic interaction, which is mainly driven by the ligand exchange of citrates to the amine groups.[9] Fig. 1c and d shows the TEM images of the obtained $DySiO_2$–$(Au)_n$ nanospheres, from which it can be seen that the hybrid nanocomposites are composed of a $DySiO_2$

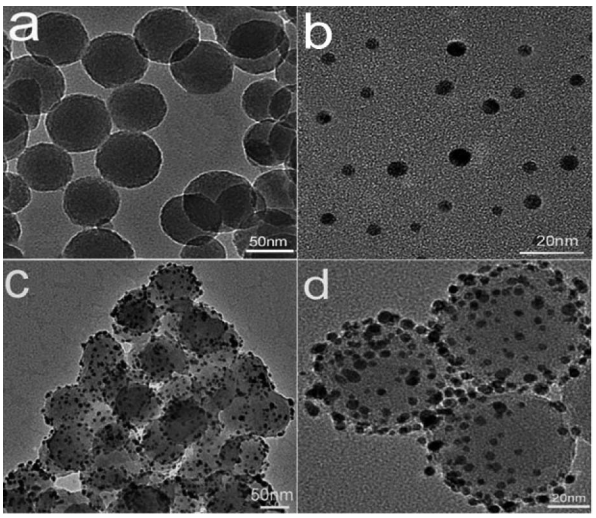

Fig. 1 TEM images of (a) Rubpy-dye-doped silica ($DySiO_2$) nanoparticles, (b) citrate-stabilized Au NPs, (c) Low- and (d) High-magnification TEM images of $DySiO_2$–$(Au)_n$ core-satellite nanospheres.

State Key Laboratory of Rare Earth Resource Utilizations, Changchun Institute of Applied Chemistry, Chinese Academy of Sciences, Changchun, 130022, China. E-mail: hongjie@ciac.jl.cn, liudp@ciac.jl.cn; Fax: +86-431-85698041; Tel: +86-431-85262127

† Electronic supplementary information (ESI) available: Details of experimental procedures. See DOI: 10.1039/c1dt10106d

core linked by roughly spherical Au nanoparticle satellites. Well-dispersed Au NPs decorate the surfaces of the nanospheres quite uniformly. Both nanoparticle components retain their initial sizes, and the overall size of the hybrid nanocomposites is approximately 70 nm. Hybrid nanocomposites are stable in aqueous media and phosphate buffer solution. TEM studies confirmed the success of the attachment of Au NPs to $DySiO_2$. Since the Au NPs are attached through a well-defined scheme that involves interaction of the sites on the surfaces decorated by amine functional groups, our decoration technique presents an excellent method for monitoring the presence of these chemical groups on the surfaces of nanospheres. It is also noted that the interaction between Au NPs and $DySiO_2$ nanospheres is quite strong, because washing does not remove them. As a control, $DySiO_2$ nanospheres (without amine modifications) are mixed with gold colloid, and almost no Au NPs are found on the nanospheres. This indicates that the amine plays a key role in the attachment; it acts as a bridge to connect Au NPs with $DySiO_2$ nanospheres.

In addition to verification of the formation of $DySiO_2$–$(Au)_n$ nanocomposites with TEM characterization, further insight into the optical changes at various stages has been carried out by UV-vis absorption and photoluminescence (PL) spectroscopy. Note that the Au NPs with sizes ranging from 5 to 20 nm in diameter have a typical absorption band at around 520 nm, known as the surface plasmon band.[10] Fig. 2a shows UV-vis absorption spectra of $DySiO_2$–$(Au)_n$, $DySiO_2$, and Au NPs. For the $DySiO_2$–$(Au)_n$ core-satellite nanospheres, the surface plasmon band shows a red-shift compared to the case of Au NPs as shown in Fig. 2a, indicating the surface absorption changed upon coating. For comparison, $DySiO_2$ NPs did not show any characteristic absorption in the selected region. A similar phenomenon was observed in Au–SiO_2 and Au–Fe_3O_4 core-shell nanocrystal systems, in which the coverage of shell materials possessing a higher refractive index led to a red-shift in the SPR position of Au.[11] Fig. 2b shows the PL spectrum of the as-synthesized $DySiO_2$–$(Au)_n$ nanocrystals compared with that of the $DySiO_2$ counterpart. The $DySiO_2$ NPs have a strong emission spectrum at 595 nm with the excitation wavelength at 458 nm, which matches well with that of free Rubpy dye.[12] Additionally, we can observe that the emission wavelength of $DySiO_2$–$(Au)_n$ nanocomposites is a little red shifted compared to $DySiO_2$ NPs alone, indicating that the fluorescence spectrum of the Rubpy dye molecule is sensitive to the chemical environment around the dye molecule.[13] Emphatically, we can observe from Fig. 2b that the existence of Au NPs is not quenching the fluorescence of the Rubpy dye-doped SiO_2 NPs greatly. These experiments indicate that the advantages of both the Au and the Rubpy dye can be retained when combining them into one sample using our core-satellite structure designing approach.

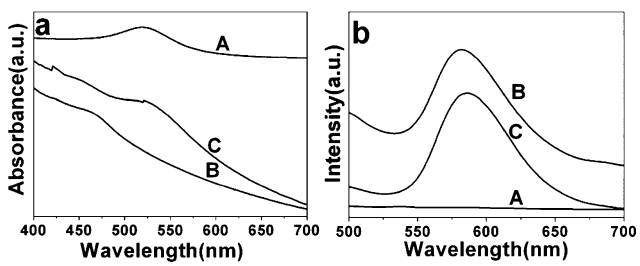

Fig. 2 (a) UV-vis absorption spectra and (b) fluorescence spectra of the as-prepared products: (A) Au nanoparticles, (B) $DySiO_2$ nanospheres, (C) $DySiO_2$–$(Au)_n$ core-satellite nanospheres.

To investigate their ability as a biolabel, the DNA modified $DySiO_2$–$(Au)_n$ nanospheres were applied in cell fluorescence imaging. We demonstrated their potential as markers for biological imaging by labeling the MCF-7 cancer cells. The thiolated DNA is covalently bound to the surface of the $DySiO_2$–$(Au)_n$ nanospheres readily *via* the self-assembled Au–S bond, resulting in DNA–$(Au)_n$–$DySiO_2$ conjugates.[14] Meanwhile, because the particles are protected by the surface-bound DNA, the particles do not covalently bond to form composite aggregates and the aggregation is reversible with sonication. Fig. 3a and b show typical labeling of MCF-7 cancer cells using such DNA-modified $DySiO_2$–$(Au)_n$ conjugates. One can see that strong orange fluorescence is observed from the $DySiO_2$–$(Au)_n$ -DNA conjugate treated MCF-7 cells (Fig. 3b), which is associated with orange emission of Rubpy-dye-doped silica NPs. Bright field measurements (Fig. 3a) after treatment with $DySiO_2$–$(Au)_n$ NPs confirm that the cells are viable throughout the imaging experiments. In contrast, Fig. 3c and d present an example of the fluorescence images of normal cells labelled with the $DySiO_2$–$(Au)_n$ NPs–DNA conjugate under a similar fluorescence microscope. As shown in Fig. 3d, no fluorescence is observed from the control HEK 293T cell. In order to further confirm the targeted images of tumor cells, Fig. 3e and f exhibit the fluorescence images of mixed cells (MCF-7 and HEK 293T), which

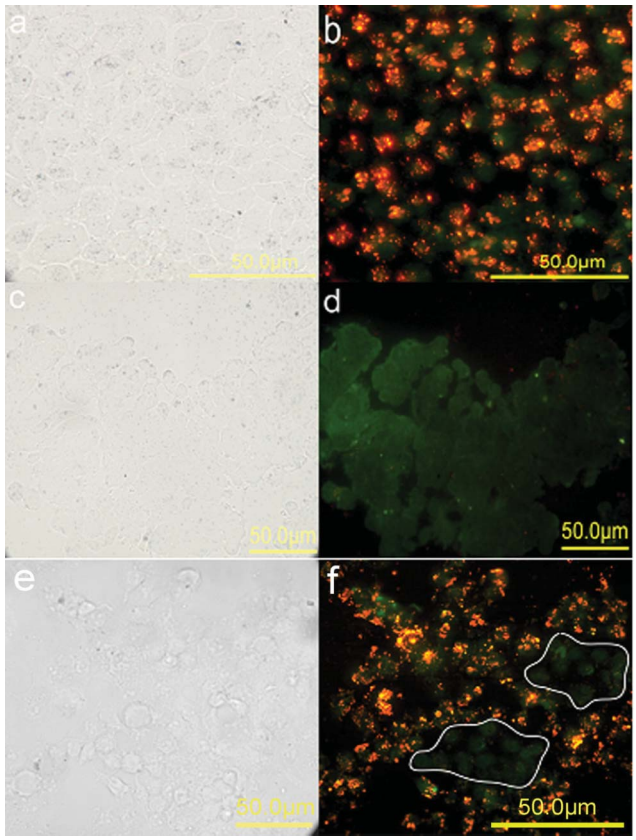

Fig. 3 (a, b) Fluorescence images of cancer cells MCF-7, (c, d) normal cells HEK 293T and (e, f) mixed cells of MCF-7/HEK 293T after treatment with 1 μg mL^{-1} $DySiO_2$–$(Au)_n$ core-satellite nanospheres for 12 h. In image f, cells inside the white circle represent HEK 293T cells and others are MCF-7 cells.

illustrate that Apt–$(Au)_n$–$DySiO_2$ conjugation binds to MCF-7 cells selectively, but not HEK 293T cells. Besides, the overlay of the bright field and fluorescence images further demonstrates that luminescence is strongly correlated with the intracellular region, suggesting that the $DySiO_2$–$(Au)_n$ NPs are internalized into the cells rather than merely staining the membrane surface. These results demonstrate that DNA conjugated $DySiO_2$–$(Au)_n$ NPs are extremely promising candidates in targeting cancer cells for imaging and detecting purposes.

For future biological applications, nanomaterials should be non-toxic or have low-cytotoxicity. As shown in Fig. 3, no signs of morphological damage to the cells are observed upon treatment with the hybrid nanocomposites, thereby demonstrating their minimal cytotoxicity. To further estimate the cytotoxicity of the $DySiO_2$–$(Au)_n$ core-satellite hybrid nanocomposites, an MTT assay was performed on MCF-7 and HEK 293T cells over a period of 24 to 48 h with a varied nanoparticle dose over a range of 0.25–25 μg mL^{-1}. From Fig. 4, one can observe that both cell lines retain more than 97% viability even in the presence of a high $DySiO_2$–$(Au)_n$ nanocomposites loading of 25 μg mL^{-1} for 24 and 48 h. The low *in vitro* cytotoxicity of the hybrid nanocomposites can be attributed to the fact that a thick layer of SiO_2 and an outer layer of biocompatible Au NPs prevent the leak of the dye molecules. The efficient labeling of the cells *in vitro* as well as low cytotoxicity even at high nanoparticle dosage prompt us to use these core-satellite-based nanoparticles for *in vivo* imaging.

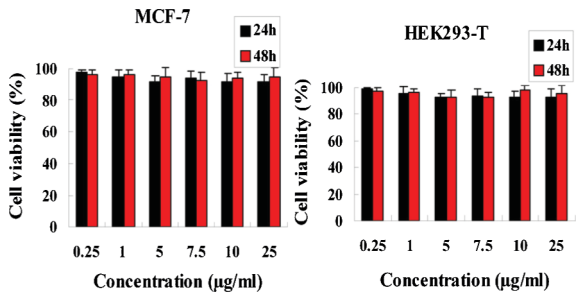

Fig. 4 Cell viability of MCF-7 (left) and HEK 293T (right) cells incubated with $DySiO_2$–$(Au)_n$ core-satellite nanospheres at varied concentrations for 24 and 48 h.

Conclusions

In summary, we have demonstrated the realization of high performance "core-satellite" structured nanoparticles containing an organic dye incorporated in the silica shell and fluorescence quenching Au nanoparticles with excellent fluorescent properties. The uniform Au nanoparticles were anchored to the surfaces of $DySiO_2$ nanospheres by a simple and versatile scheme of electrostatic adsorption. In addition, this method of decorating nanoparticles can serve as a general route for the next-generation probes in the detection and imaging of biological targets. Then the Au nanoparticles modified $DySiO_2$ nanospheres were conjugated with a nucleic acid ligand and then applied in cell imaging for cancer cell detection. The results clearly indicate that the Au functionalized $DySiO_2$ nanocomposites are extremely promising candidates for use in targeted imaging of tumor cells.

Acknowledgements

The authors are grateful to the financial aid from the National Natural Science Foundation of China (Grant Nos. 21071140) and National Natural Science Foundation for Creative Research Group (Grant Nos. 20921002).

Notes and references

1 (*a*) K. Riehemann, S. W. Schneider, T. A. Luger, B. Godin, M. Ferrari and H. Fuchs, *Angew. Chem., Int. Ed.*, 2009, **48**, 872; (*b*) A. G. Martínez, J. Pérez-Juste and L. M. Liz-Marzán, *Adv. Mater.*, 2010, **22**, 1182; (*c*) R. Alvarez-Puebla and L. Liz-Marzán, *Small*, 2010, **6**, 604.
2 (*a*) D. J. Bharali, I. Klejbor, E. Stachowiak, P. Dutta, I. Roy, N. Kaur, E. J. Bergey, P. N. Prasad and M. Stachowiak, *Proc. Natl. Acad. Sci. U. S. A.*, 2005, **102**, 11539; (*b*) I. Roy, T. Y. Ohulchanskyy, D. Bharali, H. Pudavar, R. Mistretta, N. Kaur and P. Prasad, *Proc. Natl. Acad. Sci. U. S. A.*, 2005, **102**, 279; (*c*) M. Faisal, Y. N. Hong, J. Z. Liu, Y. Yu, J. Y. Lam, A. J. Qin, P. Lu and B. Z. Tang, *Chem.–Eur. J.*, 2010, **16**, 4266.
3 (*a*) X. H. Huang, S. Neretina and M. A. El-Sayed, *Adv. Mater.*, 2009, **21**, 1; (*b*) U. H. F. Bunz and V. M. Rotello, *Angew. Chem., Int. Ed.*, 2010, **49**, 2; (*c*) E. E. Connor, J. Mwamuka, A. Gole, C. J. Murphy and M. D. Wyatt, *Small*, 2005, **1**, 325; (*d*) C. M. Goodman, C. D. Mccusker, T. Yilmaz and V. M. Rotello, *Bioconjugate Chem.*, 2004, **15**, 897; (*e*) N. Pernodet, X. Fang, Y. Sun, A. Bakhtina, A. Ramakrishnan, J. Sokolov, A. Ulman and M. Rafailovich, *Small*, 2006, **2**, 766.
4 (*a*) H. Yi, J. Leunissen, G. Shi, C. Gutekunst, S. Hersch and J. Histochem, *Cytochem.*, 2001, **49**, 279; (*b*) A. G. Tkachenko, H. Xie, Y. Liu, D. Coleman, J. Ryan, W. R. Glomm, M. K. Shipton, S. Franzen and D. L. Feldheim, *Bioconjugate Chem.*, 2004, **15**, 482.
5 (*a*) K. Y. Jiang, A. Eitan, L. Schadler, P. Ajayan and R. Siegel, *Nano Lett.*, 2003, **3**, 275; (*b*) C. G. Wang and J. Irudayaraj, *Small*, 2010, **6**, 283; (*c*) C. J. Xu, B. D. Wang and S. H. Sun, *J. Am. Chem. Soc.*, 2009, **131**, 4216.
6 (*a*) M. C. Daniel and D. Astruc, *Chem. Rev.*, 2004, **104**, 293; (*b*) P. Zhang and Y. Y. Guo, *J. Am. Chem. Soc.*, 2009, **131**, 3808.
7 (*a*) X. X. He, H. L. Nie, K. M. Wang, W. H. Tan, X. Wu and P. F. Zhang, *Anal. Chem.*, 2008, **80**, 9597; (*b*) Y. J. Song, C. Zhao, J. S. Ren and X. G. Qu, *Chem. Commun.*, 2009, 1975.
8 (*a*) J. Yang, J. Y. Lee, H. P. Too, G. M. Chow and L. M. Gan, *Chem. Phys.*, 2006, **323**, 304; (*b*) N. R. Jana, L. Gearheart and C. J. Murphy, *Langmuir*, 2001, **17**, 6782.
9 (*a*) F. Caruso, R. A. Caruso and H. Mohwald, *Science*, 1998, **282**, 1111; (*b*) D. Caruntu, B. L. Cushing, G. Caruntu and C. J. Qònnor, *Chem. Mater.*, 2005, **17**, 3398.
10 (*a*) M. C. Daniel and D. Astruc, *Chem. Rev.*, 2004, **104**, 293; (*b*) W. T. Chen, T. T. Yang and Y. J. Hsu, *Chem. Mater.*, 2008, **20**, 7204.
11 (*a*) L. M. Liz-Marzán, M. Giersig and P. Mulvaney, *Langmuir*, 1996, **12**, 4329; (*b*) V. Salgueirinõ-Maceira, F. Caruso and L. M. Liz-Marzán, *J. Phys. Chem. B*, 2003, **107**, 10990; (*c*) W. Shi, H. Zeng, Y. Sahoo, T. Y. Ohulchanskyy, Y. Ding, Z. L. Wang, M. Swihart and P. N. Prasad, *Nano Lett.*, 2006, **6**, 875.
12 (*a*) X. Zhao, R. Tapec-Dytioco and W. H. Tan, *J. Am. Chem. Soc.*, 2003, **125**, 11474; (*b*) S. Santra, K. Wang, R. Tapec and W. H. Tan, *J. Biomed. Opt.*, 2001, **6**, 160.
13 (*a*) H. Ow, D. Larson, M. Srivastava, B. Baird, W. Webb and U Wiesner, *Nano Lett.*, 2005, **5**, 113; (*b*) R. Kumar, I. Roy, T. Ohulchanskky, L. Vathy, E. Bergey, M. Sajjad and P. Prasad, *ACS Nano*, 2010, **4**, 699.
14 (*a*) X. Wang and X. Q. Guo, *Analyst*, 2009, **134**, 1348; (*b*) K. Brown, D. Walter and M. Natan, *Chem. Mater.*, 2000, **12**, 306.

